

# Influence of peak temperature during in-service welding of API X70 pipeline steels on microstructure and fracture energy of the reheated coarse grain heat-affected zones

Chaowen Li · Yong Wang · Yuhua Chen

Received: 11 October 2010 / Accepted: 25 April 2011 / Published online: 7 May 2011  
© Springer Science+Business Media, LLC 2011

**Abstract** In this investigation, thermal simulated specimens were used to investigate the effect of second peak temperature during in-service welding on characteristic fracture energy and microstructure feature of the subcritically (SC), intercritically (IC), supercritically (SCR), and unaltered (UA) reheated coarse grain heat-affected zones (CGHAZs). The API X70 high-strength pipeline micro-alloyed steel was subjected to processing during in-service welding by applying double thermal cycle shielded metal arc welding process with heat input of 9.3 kJ/cm and thermal cycles to simulate microstructure of reheated CGHAZs. This consisted of first thermal cycle with a peak temperature of 1350 °C, then reheating to different second peak temperatures of 600, 800, 1000, and 1200 °C with a constant cooling rate of 60 °C/s. Toughness of the simulated reheated CGHAZs were assessed using Charpy impact testing at –20 °C, and the corresponding fractographs, optical micrographs, and electron micrographs have been examined. It is found that accelerating cooling rate during in-service welding has an improving effect on the microstructure of CGHAZs. Owing to small heat-input and accelerating cooling, the grain size in reheated CGHAZs is relatively small and the brittle microphases are eliminated or minimized. The Charpy impact results show that the CGHAZ fracture energy is improved after the

second thermal cycle. The SC CGHAZ showed higher absorbed impact energy and the IR CGHAZ had less absorbed energy, but the phenomenon of embrittlement in IR CGHAZ is not serious. Therefore, it can be concluded that the fracture energy of CGHAZ and IR CGHAZ can be improved by accelerating cooling with appropriate cooling rate.

## Introduction

In order to reduce the transportation cost in the commercialization of remote oil and natural gas resources, the development tendency and prospect of pipeline steel is to refine acicular ferrite microstructure with high-strength and optimum toughness for new micro-alloyed high-strength low-alloy (HSLA) steels, produced by advanced manufacture process of the thermo-mechanical controlled rolling (TMCR) process. The excellent fracture properties of the base material must be carefully reconsidered because, as well-accepted, welding can considerably alter the metallurgical and mechanical properties of materials and generally causes degradations of the properties. Therefore, recent research focuses on the toughness property of high-strength micro-alloyed steels [1–7].

The balance of high-strength and good toughness can be upset by the multiple thermal cycles during in-service welding of long-distance high pressure oil and natural gas pipelines. It is known that the multipass welding operation may lead to grain refinement in under passes as they are reheated resulting from the multipass welding. It also forms local brittle zones (LBZs) which decreases the toughness value and results in brittle fracture of the multipass welded joints [8]. In regions that are subjected to reheating, the coarse grain heat-affected zone (CGHAZ) adjacent to the fusion line has the lowest

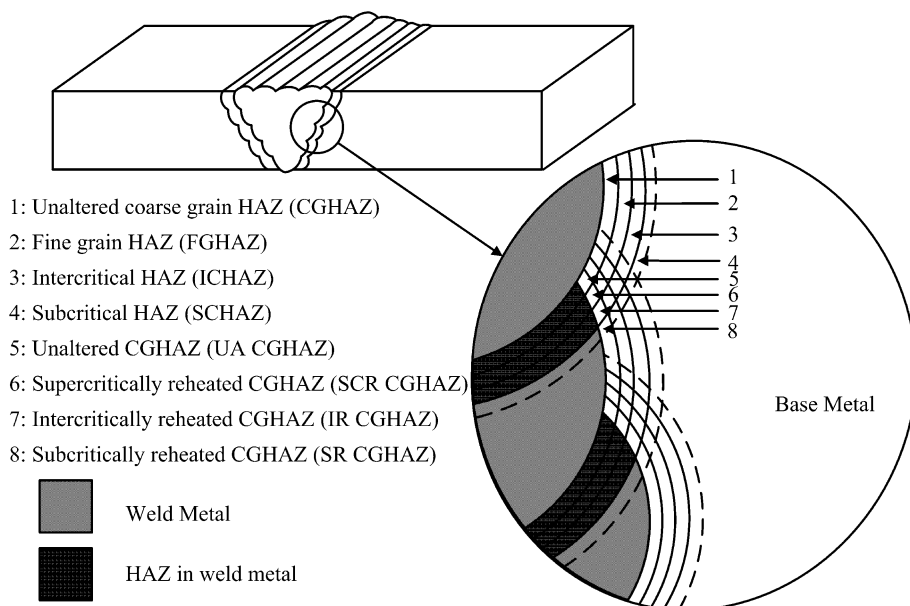
C. Li · Y. Wang · Y. Chen  
College of Mechanical and Electronic Engineering,  
China University of Petroleum, Dongying 257061,  
People's Republic of China

Y. Wang (✉)  
School of Mechanical and Electronic Engineering,  
China University of Petroleum, Dongying 257061, Shandong,  
People's Republic of China  
e-mail: yongwang@upc.edu.cn

toughness among the various regions within the heat-affected zone (HAZ) because of unfavorable microstructure such as large prior-austenite grain size [9, 10]. The various regions of a HAZ multipass weld in pipeline steel are defined in Fig. 1. The complicated metallurgy is a direct result of the overlapping thermal profiles. Although Fig. 1 shows a multipass weld, only single and double thermal cycle areas are depicted. While this is sufficient for the purpose of this article, it should be noted that triple-cycle microstructures are significant and have been studied in relation to LBZs [7, 11]. Metallographic analyses reveal that a CGHAZ can be roughly categorized into four characteristic zones according to the peak temperature of subsequent thermal cycles in a multipass welding procedure: (i) unaltered CGHAZ (UA CGHAZ), the region reheated above specific temperature of grain growth or not reheated at all, (ii) supercritically reheated CGHAZ (SCR CGHAZ), the region reheated above  $A_{C3}$ , (iii) intercritically reheated CGHAZ (IR CGHAZ), the region reheated between  $A_{C1}$  and  $A_{C3}$ , and (iv) subcritically reheated CGHAZ (SR CGHAZ), the region reheated below  $A_{C1}$  [12]. Many studies have been conducted on microscopic fracture characteristics in these CGHAZs for the pipeline steels by large heat input [13–16]. However, for in-service welding of pipeline with small heat input and accelerating cooling rate, there have been few studies on the microstructures and fracture behaviors of the CGHAZs, and far fewer research are available for API X70 pipeline steel HAZ.

This study is devoted to use the results of Charpy impact tests and scanning electron microscopy (SEM) observations. Then, the effects of microstructural change on the fracture behaviors are proposed by the metallurgical analysis.

**Fig. 1** Schematic representation of various HAZ regions in a multipass weld



## Experimental procedures

### Experimental material

The experimental material was obtained from API X70 pipeline steel with a diameter 1 016 mm and thickness of 14.4 mm, which was used in the Chinese West-East Natural Gas Transporting project. The chemical composition of this steel is shown in Table 1. The critical temperatures were calculated from the empirical formula of Andrew [17], and the temperature of  $A_{C1}$  and  $A_{C3}$  is shown in Table 2.

### Reproduced heat cycle tests

Because of the small physical size of the HAZ, taking suitable specimens from component welds is not always possible and so attempts have been made to simulate the metallurgical structures in such HAZ areas in larger specimens by appropriate heat treatment. Since simulated HAZ tests give the same toughness ranking, although not the same absolute values [16], as those on actual welding HAZ, a simulated reheated CGHAZ can be used to substitute actual multipass welding.

The thermal cycle simulation was performed with a Gleeble1500 thermo-mechanical simulator. Rectangle bar specimens ( $10.5 \times 10.5 \times 80 \text{ mm}^3$ ) for thermal cycle simulation were cut in longitudinal direction with respect to rolling direction. A schematic illustration of the simulation profile is shown in Fig. 2. The thermal cycle for weld simulation is generally characterized both by the peak temperature ( $T_p$ ) and the cooling time from 800 to 500 °C

**Table 1** Chemical composition of investigated steel (wt%)

Elements	Content
C	0.05
Si	0.26
Mn	1.48
S	0.003
P	0.012
Cr	0.027
Mo	0.17
Cu	0.22
V	0.052
Ni	0.15
Ti	0.016
Nb	0.05
Pcm	0.164
Ceq	0.404

Note  $P_{cm} = C + (Mn + Cu + Cr)/20 + Mo/15 + V/10 + Si/30 + Ni/60$

$C_{eq} = C + (Mn + Si)/6 + (Ni + Cu)/15 + (Cr + Mo + V)/5$

**Table 2** Critical temperatures of investigated steel (°C)

$A_{C1}$	$A_{C3}$
732	887

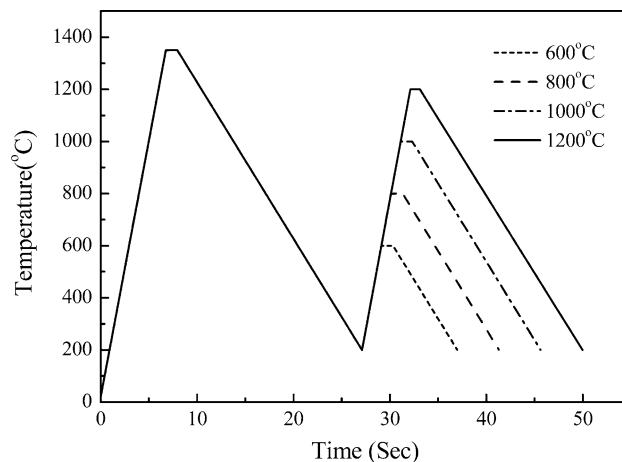
Note  $A_{C1} = 723 - 10.7Mn - 3.9Ni + 29Si + 16.7Cr + 290As + 6.38W$

$A_{C3} = 910 - 230C^{0.5} - 15.2Ni + 44.7Si + 104V + 31.5Mo + 13.1W$

( $\Delta t_{8/5}$ ) or from 500 to 300 °C ( $\Delta t_{5/3}$ ), and  $\Delta t_{5/3}$  is used when  $T_p$  is below 800 °C. The specimen temperature was controlled with a type-K thermocouple wire percussion welded at the midsection. The specimens were heated to the first peak temperature at 1350 °C (taken as 1350 °C for the CGHAZ) at a linear rate of 200 °C/s. Then, the specimens were cooled down with the constant cooling time ( $\Delta t_{8/5}$ ) of 5 s and the cooling rates were approximately equivalent to that in-service welding of pipeline steel by shielded metal arc welding (SMAW) with heat input of 9.3 kJ/cm and weld efficiency 0.68, in 8 mm thick plate. The peak temperature of the second weld thermal cycle,  $T_{p2}$ , was varied between 600 and 1200 °C for simulating the different regions in HAZ. The cooling rates of the second thermal cycle were the same as that of the first thermal cycle.

#### Microstructure examination

In order to characterize the microstructure of the base metal and the CGHAZs, the optical micrographic specimens, were prepared by conventional grinding and polishing techniques

**Fig. 2** Typical simulation profile for double thermal cycles when the cooling rate is maintained constant during the cycles

and etched with 4% Nital solution for reveal of the microstructure. The microstructural features were observed with an NIKON EPIPHOT 300U OM. A few samples were etched in Lepera's reagent (1 part of 1 mL sodium metabisulfite in 100 mL distilled water and 1 part of 4 mL picric acid in ethanol) in addition to Nital etching to confirm the presence of M-A constituent under the optical microscope. TEM work was also carried out on a few samples by using thin foils, which were taken from the transverse cross-section planes of the steel plates, mechanically thinned from 300 to 50 μm, polished by the precision ion polishing system with the type GL-6960. The thin foils were examined on an H-800 TEM operating at 150 kV.

#### Measurement of mechanical properties

Hardness tests and Charpy impact tests were performed on the specimens that had been subjected to heat cycle. In the hardness test, a Vickers pyramidal indenter with an indenting load of 98 N was applied to the centre cross-sectional surface of a specimen that had been subjected heat cycle. The average of the measurement values found at five measurement points on the cross-sectional surface was taken as the hardness.

After the welding thermal cycle was applied, specimen was subjected to the Charpy impact test to find the fracture energy of the simulated CGHAZs. V-notch Charpy impact tests were carried out on subsize Charpy bars with a  $10 \times 10 \times 55$  mm<sup>3</sup> size at specified position parallel to the specimen central line on a JB-30B Charpy impact test machine according to GB/T229-1994. The absorbed energy value was measured at the temperature of –20 °C. Four specimens were tested for each condition, and average values were used for this study. Since the simulated specimens for each condition had a single microstructure, there was little scatter of impact values for a given condition.

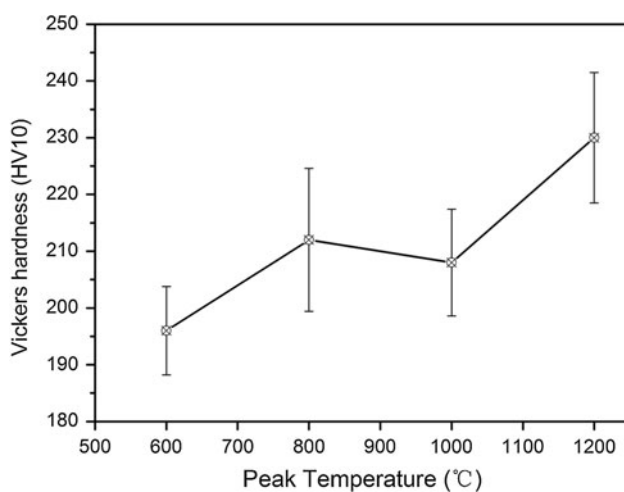


**Fig. 3** Variation of Vickers hardness with the second peak temperature

## Experimental results

### Hardness level and low temperature impact energy

Figure 3 shows the results of measurements of the Vickers hardness (HV10) under a load of 98 N. All the simulated reheated CGHAZ showed Vickers hardness around HV230. Hardness across the UA CGHAZ and IR CGHAZ has been a concern as high hardness levels correlate with preferential corrosion, and hydrogen-induced cracking either during welding or from sour gas.

As such a limit of Vickers 250 (HV 250) has traditionally been placed on line pipe, but is extended to HV270 or even HV290 for higher strength grades in non-sour service [18]. It can be seen from Fig. 3, that hardness in all CGHAZs meets the proposed limit of HV290.

The results of Charpy V-notch impact tests are shown in Fig. 4, with respect to the second peak temperature. When the peak temperature of second thermal cycle is 800 °C, the toughness of the primary CGHAZ is not

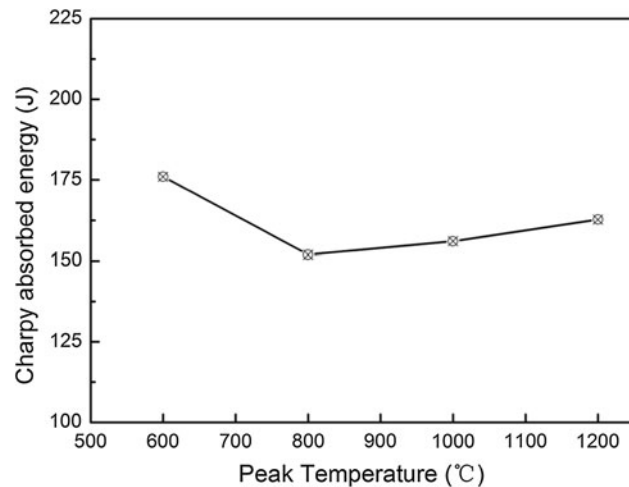


**Fig. 4** Variation of Charpy absorbed energy with the second peak temperature

improved. The IR CGHAZ has the lower absorbed energy than the other peak temperatures. The SC CGHAZ has higher absorbed energy. Although the Charpy impact energy of the specimens at –20 °C were lower than 252 J of the base metal, all specimens exhibited moderate fracture energy near 150 J. Also, no clear tendency of change in toughness with the peak temperature of the second thermal cycle was found. Therefore, it was concluded that there was no LBZ in the CGHAZs at –20 °C during in-service welding.

### Effect of peak temperature on microstructure

Figure 5a and b presents the optical micrographs of base metal (BM) and CGHAZ of API X70 pipeline steel, respectively. It can be seen that the microstructure of the BM (Fig. 5a) is acicular ferrite with quasi-polygonal ferrite dominated microstructures. The mean grain size is about 15 µm and the minimal grain is 3–5 µm. After undergoing a thermal cycle with the peak temperature of 1350 °C, the

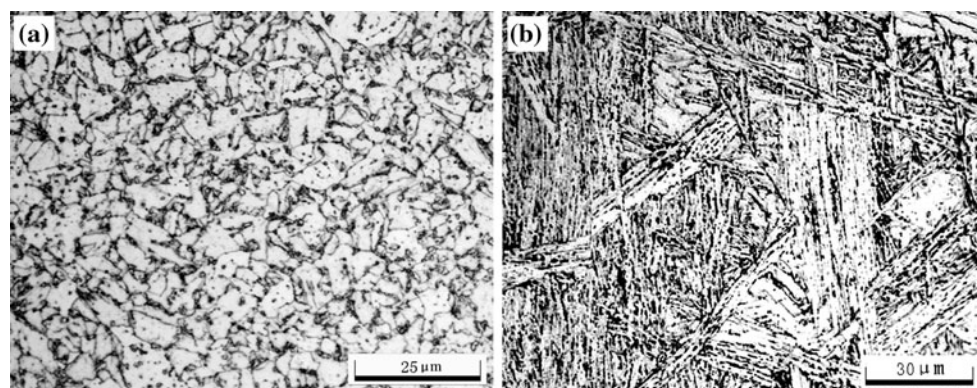


**Fig. 5** Optical micrographs showing the tested steel microstructure, **a** BM, **b** CGHAZ

microstructure changes into granular bainite with lath bainite dominated microstructures. In CGHAZ (Fig. 5b), the coarse grain size was formed by heat cycles effects. The laths are slender and have regular arrangement.

Owing to multiple thermal cycles during the welding of the structural steel, the HAZ is formed according to various precipitate mechanisms and phase transformations. As a result, the metallurgical heterogeneity in HAZ is clearly recognized. It is possible to determine the distribution of typical microstructures by a surface analysis of the isothermal lines.

Figure 6 shows the optical micrographs of the sub-zones in the CGHAZ simulated using different peak temperatures. The microstructure of the 1350 °C being reheated with the peak temperature of 600 °C (Fig. 6a) has no great difference with that of the CGHAZ. The reason is that the peak temperature of second thermal cycle is low and there is no phase transformation in the original CGHAZ. The IR CGHAZ was a partially transformed region, where part of the microstructure was transformed into austenite in the reheating thermal cycles. The austenite grain size was coarse and the microstructure had irregular arrangement, as shown in Fig. 6b. At the peak temperature of 1000 °C (Fig. 6c), a significant content of granular bainite was formed because of complete recrystallization. With

subsequent increase in peak temperature, the austenite grain size was increased. At 1200 °C, the microstructure primarily consisted of granular bainite together with bainitic lath with the original austenite grains of average grain size of 55 μm (Fig. 6d).

As the M–A constituent forms during bainite transformation; the carbon-enriched, untransformed regions will partially transform into martensite at low temperature. The carbon-enriched austenite regions formed by rejecting of carbon from ferrite to austenite following the transformation of bainite ferrite. The formation of M–A constituents leads to the decrease of Charpy impact energy in the weld HAZ. Morphology of M–A constituent investigation was carried out by both optical and transmission electron microscopes.

Typical OM microstructures observed are shown in Fig. 7. Carbides are observed as dark particles and M–A constituents are observed as white constituents in these micrographs. The morphology of M–A constituent is semicontinuous elongated rods. In general, the presence of M–A constituents shows approximately parallel and regular distribution. However, the size of M–A constituent in the IR CGHAZ is coarser than that in the CGHAZ.

The morphology of M–A constituent was also examined using TEM. Example showing the TEM microstructures of

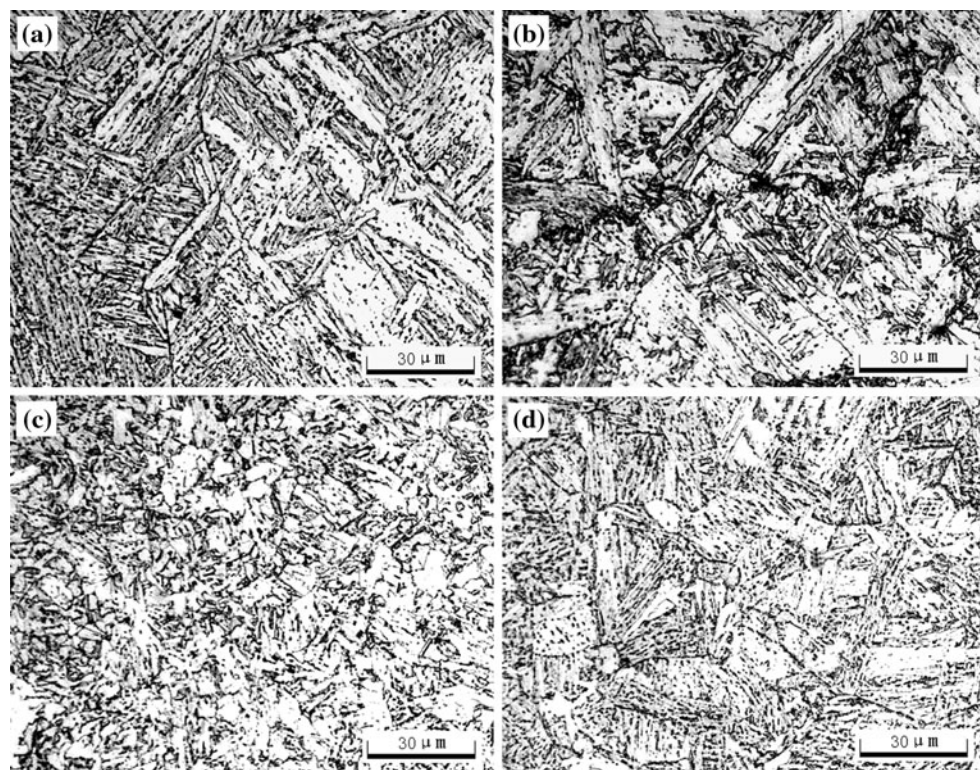


**Fig. 6** Optical micrographs showing the microstructure of simulated specimens, **a** SR CGHAZ, **b** IR CGHAZ, **c** SCR CGHAZ, **d** UA CGHAZ

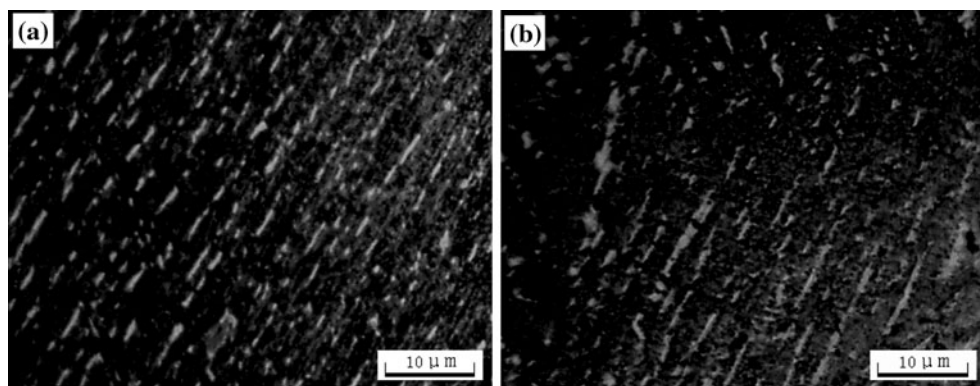


**Fig. 7** Optical micrographs after etching with Lepera's reagent, **a** CGHAZ, **b** IR CGHAZ

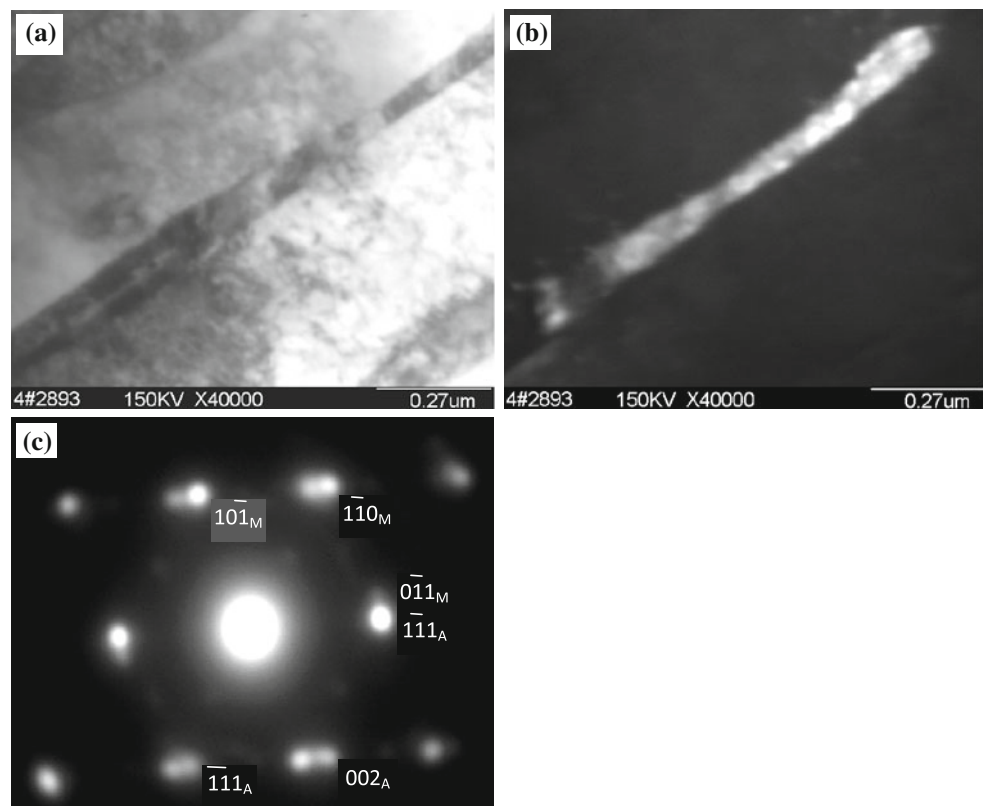


**Fig. 8** Typical structure of M–A constituent, **a** bright field of M–A constituent, **b** dark field of M–A constituent, **c** micro-diffraction pattern of M–A constituent

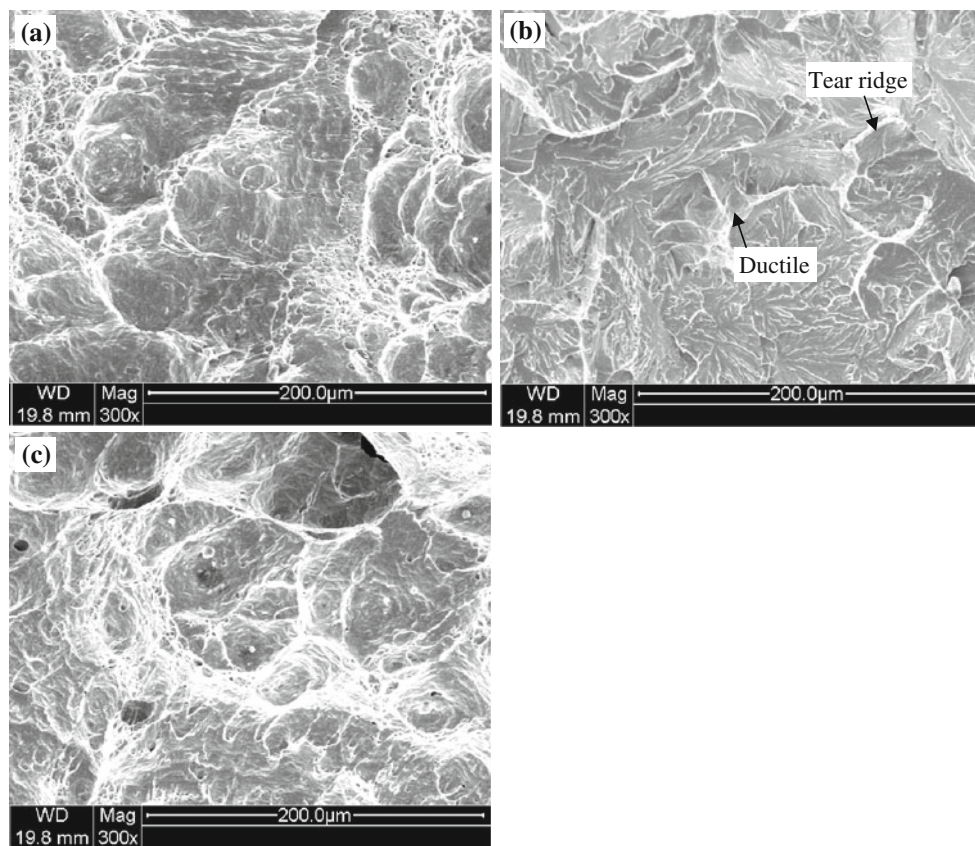
M–A constituent and its micro-diffraction pattern are given in Fig. 8. The rod-like M–A particles were mostly along polygonal ferrite boundaries and the bainite lath boundaries.

#### Fracture morphology

Fracture surfaces of the sub-zones in the CGHAZ simulated using different peak temperatures were examined using the SEM to determine the fracture morphology.

The fractographs of the tested specimens at –20 °C are shown in Fig. 9. From the fractographs, it is easily seen that ductile fracture is present in the SR CGHAZ and SCR CGHAZ specimens. On the other hand, the IR CGHAZ specimens with the lowest impact value fracture by the mixed mode of localized ductile dimple rupture and mainly quasi-cleavage. This change in fracture mode is consistent with the change in Charpy impact energy. Owing to small heat-input welding and accelerating cooling rate, the

**Fig. 9** SEM fractograph of Charpy impact simulated specimens, **a** SR CGHAZ, **b** IR CGHAZ, **c** SCR CGHAZ



effective grain size in the reheated CGHAZs for in-service welding is smaller than that in high heat-input welding, which has an effect in toughness improvement. High density of piled-up dislocations at grain boundary and sub grain boundary can collapse into a microcrack to open up the crack and increase driving force for crack propagation into ferrite matrix. Owing to increase of dislocations, small grain size and area fraction of secondary phases, the phenomenon of embrittlement in IR CGHAZ is not serious.

## Conclusions

In this study, the authors have studied the influence of peak temperature on microstructure and fracture energy of the reheated CGHAZs during in-service welding of API X70 pipeline steels. It is shown that the main microstructure is all granular bainite and lath bainite, and the difference is in the amount and size of each microstructure. In addition, the Charpy impact energy of CGHAZs is improved after the second thermal cycle except IR CGHAZ. The fracture energy didn't deteriorate drastically for the partially transformed HAZ may be related with the formation of mixture microstructure, in which the size of martensite-austenite (M-A) constituent is small and the content of M-A constituent is

relatively little for the effect of accelerating cooling. Therefore, the phenomenon of embrittlement in IR CGHAZ is not serious.

**Acknowledgements** The research was partially supported by the National Natural Science Foundation of China (51074174) and the Innovation Fund for Doctors of China University of Petroleum (B2009-13).

## References

- Shin SY, Hwang B, Lee S, Kim NJ, Ahn SS (2007) Mater Sci Eng A 458(1–2):281. doi:[10.1016/j.msea.2006.12.097](https://doi.org/10.1016/j.msea.2006.12.097)
- Corbett K, Bowen R, Petersen C (2004) Int J Offshore Polar Eng 14(1):105
- Koo JY, Luton MJ, Bangaru NV, Petkovic RA, Fairchild DP, Petersen CW, Asahi H, Hara T, Terada Y, Sugiyama M, Tamehiro H, Komizo Y, Okaguchi S, Hamada M, Yamamoto A, Takeuchi I (2004) Int J Offshore Polar Eng 14(1):10
- Xiao F-R, Liao B, Shan Y-Y, Qiao G-Y, Zhong Y, Zhang C, Yang K (2006) Mater Sci Eng A 431(1–2):41. doi:[10.1016/j.msea.2006.05.029](https://doi.org/10.1016/j.msea.2006.05.029)
- Lee CH, Bhadeshia HKD H, Lee HC (2003) Mater Sci Eng A 360(1–2):249. doi:[10.1016/s0921-5093\(03\)00477-5](https://doi.org/10.1016/s0921-5093(03)00477-5)
- Pan T, Yang ZG, Zhang C, Bai BZ, Fang HS (2006) Mater Sci Eng A 438–440:1128. doi:[10.1016/j.msea.2006.02.078](https://doi.org/10.1016/j.msea.2006.02.078)
- Ju J-B, Lee J-S, Jang J-i (2007) Mater Lett 61(29):5178. doi:[10.1016/j.matlet.2007.04.007](https://doi.org/10.1016/j.matlet.2007.04.007)
- Zhou Z, Liu S (1998) Acta Metall Sin Engl Lett 11(2):87

9. Lee S, Kim B, Kwon D (1992) Metall Mater Trans A 23(10):2803. doi:[10.1007/bf02651759](https://doi.org/10.1007/bf02651759)
10. Li Y, Crowther D, Green M, Mitchell P, Baker T (2001) Isij Int 41(1):46
11. Bayraktar E, Kaplan D (2004) J Mater Process Tech 153–154:87. doi:[10.1016/j.jmatprotec.2004.04.021](https://doi.org/10.1016/j.jmatprotec.2004.04.021)
12. Jang J-i, Ju J-B, Lee B-W, Kwon D, Kim W-S (2003) Mater Sci Eng A 340(1–2):68. doi:[10.1016/s0921-5093\(02\)00190-9](https://doi.org/10.1016/s0921-5093(02)00190-9)
13. Suzuki S, Kamo T, Komizo Y (2009) Weld Int 23(6):397
14. Yang Z, Sista S, Elmer JW, DebRoy T (2000) Acta Mater 48(20):4813. doi:[10.1016/s1359-6454\(00\)00279-2](https://doi.org/10.1016/s1359-6454(00)00279-2)
15. Sun W, Wang G, Zhang J, Xia D, Sun H (2009) J Mater Sci Technol 25(06):857
16. Qiu H, Mori H, Enoki M, Kishi T (2000) Metall Mater Trans A 31(11):2785
17. Andrews KW (1965) J Iron Steel Inst 203:721
18. John P (2002) In: Leigh F (ed) X80 pipeline cost workshop, Hobart